

Proton-Regulated Catalytic Activity of Nanozymes for Dual-Modal Bioassay of Urease Activity

Mingwang Liu, Guojuan Chen, Ying Qin, Jinli Li, Liuyong Hu,* Wenling Gu,* and Chengzhou Zhu*



Cite This: *Anal. Chem.* 2021, 93, 9897–9903



Read Online

ACCESS |



Metrics & More



Article Recommendations

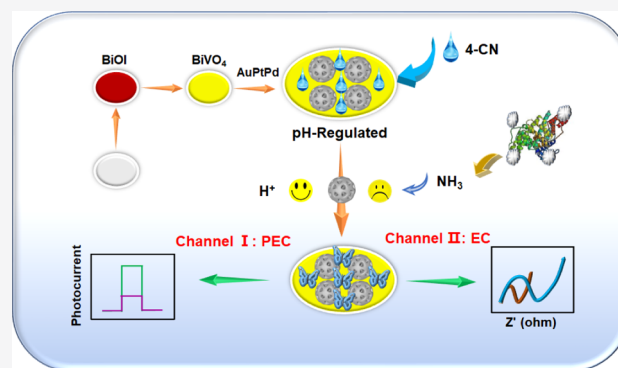


Supporting Information

ABSTRACT: Benefiting from the merits of high stability and superior activity, nanozymes are recognized as promising alternatives to natural enzymes. Despite the great leaps in the field of therapy and colorimetric sensing, the development of highly sensitive nanozyme-involved photoelectrochemical (PEC) biosensors is still in its infancy. Specifically, the investigation of multifunctional nanozymes facilitating different catalytic reactions remains largely unexplored due to the difficulty in synergistically amplifying the PEC signals. In this work, mesoporous trimetallic AuPtPd nanospheres were synthesized with both efficient oxidase and peroxidase-like activities, which can synergistically catalyze the oxidation of 4-chloro-1-naphthol to produce benzo-4-chlorohexadienone precipitation on the surface of photoactive materials, and thus lead to the decreased photocurrent as well as increased charge-transfer resistance. Inspired by the proton-dependent catalytic activity of nanozymes, a self-regulated dual-modal PEC and electrochemical bioassay of urease activity was innovatively established by in situ regulating the activity of AuPtPd nanozymes through urease-mediated proton-consuming enzymatic reactions, which can remarkably improve the accuracy of the assay. Meanwhile, the determination of urease activity in spiked human saliva samples was successfully realized, indicating the reliability of the biosensor and its application prospects in clinical diagnosis.

INTRODUCTION

Urease, as the earliest discovered nickel metalloenzyme, has attracted extensive research interest for a long time since being separated from the crystalline protein.^{1,2} Urease plays a critical role in various metabolisms of organisms, which can catalyze the decomposition of urea into ammonia and CO₂.³ Many urinary and gastrointestinal diseases including cancer and pyelonephritis are closely related to urease activity,⁴ and the sensing of urease activity has been used to diagnose some diseases.⁵ Noteworthy, the urease activity in the oral cavity is recognized as an important diagnostic biomarker for early disease diagnosis.⁶ Up to date, various methods such as fluorescence,⁷ ELISA,⁸ electrochemistry,⁹ and colorimetric^{10,11} were applied for the analysis of urease. Nevertheless, the development of an advanced functional dual-modal photoelectrochemical (PEC) and electrochemical (EC) sensing platform remains meaningful for urease detection. Recently, PEC analysis, as a novel and promising analysis technique, exhibits the merits of low cost, simple operation, antibackground interference, high sensitivity, and miniaturization, and provides great opportunities for fast and real-time detection.^{12–34} To realize a highly sensitive PEC biosensing, some effective signal amplification strategies have been developed, such as enzymatic reactions,³⁵ the steric effect,¹³ energy transfer,³⁶ and the quenching effect.³⁷ Among them, PEC



enzymatic biosensors, which combine the selectivity of enzymes and the sensitivity of PEC bioanalysis, are deemed to promote their further advancements.^{38,39} However, natural enzymes usually suffer from the disadvantages of high cost, poor stability, and storage difficulties, which limit their widespread applications.^{40–44} Moreover, enzyme immobilization on the surface of a photoelectrode will inevitably hinder the electron transfer and mass exchange during the PEC process due to the insulating characteristics of natural enzymes. To overcome these shortcomings, nanozymes, as promising artificial enzymes, have been developed as alternatives to natural enzymes due to low cost and high stability.^{15,45–50} For example, ZnFe₂O₄ nanozymes,⁴⁷ silver iodide chitosan nanoparticles,⁴⁵ and Au@CuS-GR⁴⁸ were used as peroxidase mimics to construct PEC biosensors. Despite the great advantages of PEC nanozymatic biosensors, the investigation of multifunctional nanozymes, which can

Received: May 11, 2021

Accepted: June 29, 2021

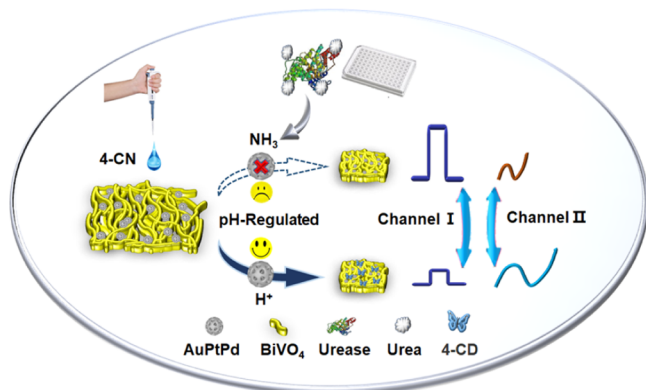
Published: July 9, 2021



facilitate different varieties of catalytic reactions, remains largely unexplored due to the difficulty in synergistically amplifying the PEC signals. Furthermore, dual-modal sensing platforms with advanced functions are greatly expected to improve the accuracy of an assay. Therefore, finely modulating the functionality of nanozymes will provide great prospects for further exploring their corresponding applications in PEC and EC dual-modal biosensing.

In this work, trimetallic AuPtPd mesoporous nanospheres were rationally designed, which displayed both excellent oxidase and peroxidase-like activities. After the immobilization of AuPtPd nanozymes on the surface of photoactive BiVO₄, no obvious recession of photocurrent was observed, manifesting the superiority of nanozymes in PEC biosensing. Owing to the remarkable oxidase and peroxidase-like activities of AuPtPd nanozymes, biocatalytic precipitation could be synergistically produced on the surface of a photoelectrode to trigger the significant photocurrent variation and increased charge-transfer resistance (R_{ct}) in the presence of H₂O₂ and 4-chloro-1-naphthol (4-CN). Inspired by the proton-dependent catalytic activity of nanozymes, a self-regulated dual-modal bioassay based on PEC and EC methods for the evaluation of urease activity was innovatively designed by in situ regulating the activity of AuPtPd nanozymes through urease-mediated proton-consuming enzymatic reactions (Scheme 1). As

Scheme 1. Mechanism of Dual-Modal PEC and EC Biosensor Based on AuPtPd Nanozymes and BiVO₄ for Urease Detection



expected, the multifunctional AuPtPd nanozyme-based dual-modal biosensor exhibits outstanding selectivity, good repeatability, and promising applicability to real sample detection.

EXPERIMENTAL SECTION

Synthesis of Mesoporous Trimetallic AuPtPd Nanospheres. The mesoporous trimetallic AuPtPd nanospheres were synthesized by a typical method with some modification.^{51–53} First, 4.8 mL of 0.02 M K₂PtCl₄, 1.6 mL of 0.02 M Na₂PdCl₄ (Na₂PdCl₄ was prepared by dissolving PdCl₂ in sodium chloride solution), 1.6 mL of 0.02 M HAuCl₄, and 100.0 μ L of 6.0 M HCl were mixed to form a homogeneous solution. Then, 80.0 mg of Pluronic F127 was added to the above solution under sonication. After the Pluronic F127 was completely dissolved in the solution, 8.0 mL of the 1.5 mM ascorbic acid (AA) solution was added to the solution immediately. The mixed solution was kept in a water bath at 40 $^{\circ}$ C for 6 h under continuous stirring. Finally, the product

was collected by centrifugation at 8000 rpm for 5 min and the residual Pluronic F127 was removed by five consecutive washing/centrifugation cycles with ultrapure water. After vacuum drying at 60 $^{\circ}$ C for 12 h, AuPtPd nanospheres were obtained.

Oxidase and Peroxidase-like Activities of the AuPtPd Nanospheres. To verify the oxidase-like activity of AuPtPd nanospheres, 3,3',5,5'-tetramethylbenzidine (TMB) was used as a chromogenic substrate. Specifically, 10 μ L of 0.5 mg mL⁻¹ of AuPtPd was added to 150 μ L of acetate buffer solution with different pH values (pH range from 3 to 9), to which 50 μ L H₂O and 50 μ L TMB (1 mM) were added. After being kept at 37 $^{\circ}$ C for 15 min, the resulting mixed solution was investigated by UV-vis scanning using a multimode reader. Similarly, 50 μ L of 10 mM H₂O₂ was used instead of water to evaluate the peroxidase-like activity of AuPtPd. The oxidase and peroxidase-like activities were assessed by monitoring the absorbance value at 652 nm.⁵⁴ The steady-state kinetic assays of oxidase-like were performed at 37 $^{\circ}$ C in NaAc buffer containing 0.1 mg mL⁻¹ AuPtPd and various concentrations of TMB. All measurements were monitored by the absorbance change at 652 nm. The kinetic parameters were calculated using the Michaelis–Menten equation: $v = V_{max} \times [S]/(K_m + [S])$, where v is the initial velocity, $[S]$ represents the substrate concentration, V_{max} is the maximal velocity, and K_m represents the Michaelis–Menten constant.

Synthesis of BiVO₄ and BiVO₄-AuPtPd Photoelectrodes. BiVO₄ photoelectrodes were prepared according to the previous report.⁵⁵ Preparation of the electroplating solution: the pH of 50 mL mixed solution containing 0.04 M Bi(NO₃)₃·5H₂O and 0.4 M KI was adjusted to 1.7 with HNO₃; then 20 mL of the ethanol solution containing 0.23 M benzoquinone was slowly added to the solution. After the pH became stable, a typical three-electrode system of an ITO working electrode (WE), an Ag/AgCl (4 M KCl) reference electrode (RE), and a platinum counter electrode (CE) was used for electrodeposition with a CHI 760D EC workstation at -0.1 V versus Ag/AgCl under vigorous magnetic stirring. The duration of the electrodeposition was around 5 min and the current density–time curve of BiOI during electrodeposition is displayed in Figure S1. Afterward, 50 mL dimethyl sulfoxide solution containing 0.08 M VO(acac)₂ was evenly dropped onto the surface of the BiOI electrode (1.0 \times 1.0 cm²) before thermal treatment in air at 450 $^{\circ}$ C for 2 h (ramp rate 2 $^{\circ}$ C min⁻¹). The BiVO₄ photoelectrodes can be obtained after being placed in 1 M NaOH solution to remove excess V₂O₅. The electrodes were then thoroughly rinsed with ultrapure water, blow-dried with nitrogen, and stored in a dry place for further use. 30 μ L AuPtPd aqueous solution (0.2 mg mL⁻¹) was dropped onto the surface of the BiVO₄ electrode, and then vacuum dried at 50 $^{\circ}$ C for 6 h to obtain BiVO₄-AuPtPd photoelectrodes.

Dual-Modal PEC and EC Detection of Urease Activity. First, 240 μ L of the mixed solution including 50 μ L urea solution (20 mM), 90 μ L urease reaction buffer (acetate buffer, 5 mM, pH 4.0), and 100 μ L various amounts of urease (0–3000 mU mL⁻¹) were added in a 96-well plate and incubated at 37 $^{\circ}$ C for 30 min. Then, 50 μ L 4-CN (1 mM) and 20 μ L H₂O₂ (10 mM) were added to the above solution and mixed evenly. Finally, the above mixture (30 μ L) was dropped on the surface of the BiVO₄-AuPtPd photoelectrode and incubated at 37 $^{\circ}$ C for 30 min. PEC measurements were carried out using a CHI 842D EC

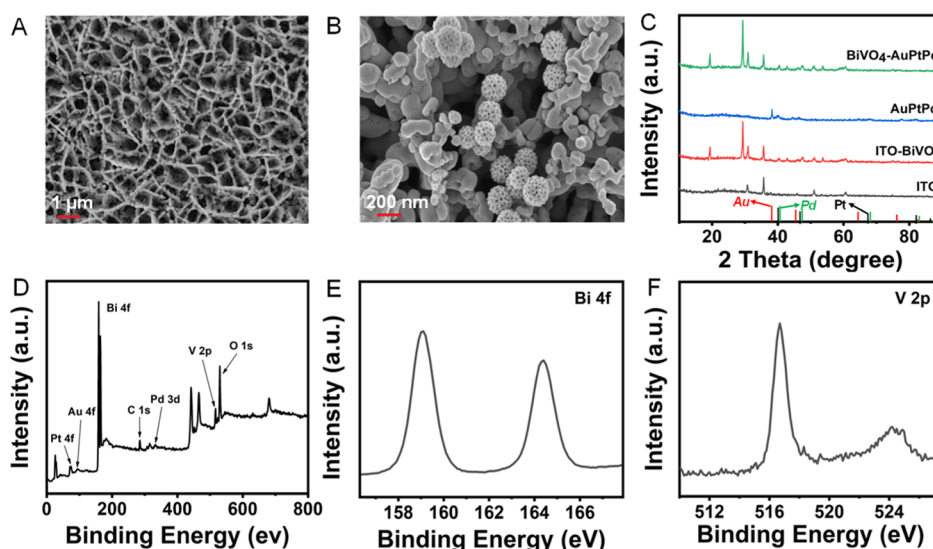


Figure 1. SEM images of BiVO_4 (A) and $\text{BiVO}_4\text{-AuPtPd}$ (B). (C) XRD patterns of BiVO_4 , AuPtPd, and $\text{BiVO}_4\text{-AuPtPd}$. (D) XPS survey spectrum of $\text{BiVO}_4\text{-AuPtPd}$. (E) Bi 4f in $\text{BiVO}_4\text{-AuPtPd}$. (F) V 2p in $\text{BiVO}_4\text{-AuPtPd}$.

workstation in a standard three-electrode configuration with the as-synthesized electrode used as the WE, a platinum wire as the CE, and an Ag/AgCl (saturated with KCl) electrode as the RE. All PEC measurements were performed at phosphate buffer solution (PBS, 0.1 M, pH 7.0) containing 1.5 mM AA at 0 V. R_{ct} was obtained by electrochemical impedance spectroscopy (EIS) under the same reaction conditions. EIS was measured on a CHI 660E EC workstation (Shanghai Chenhua Apparatus Corporation, China) with a three-electrode system in 1 M KCl solution containing the 5 mM $\text{K}_3[\text{Fe}(\text{CN})_6]/\text{K}_4[\text{Fe}(\text{CN})_6]$ (1:1) mixture as the electrolyte in a frequency range of 0.1 Hz–100 kHz.

Analysis of Urease in the Real Human Saliva Sample.

Saliva samples were collected from a healthy volunteer with informed consent. Samples were 10-fold diluted with ultrapure water to avoid interference, and the pH of the saliva sample was adjusted to 7.0. Then, the saliva sample was used to prepare urease solution in different concentrations with a volume of 100 μL . Finally, the spiked samples can be obtained by adding 90 μL reaction buffer (acetate buffer solution, 5 mM, pH 4.0) into the above solution.

RESULTS AND DISCUSSION

Design and Characterization of the Resultant Materials. Noble metal-based nanomaterials have been demonstrated promising enzyme-like catalytic activity. To realize a nanozyme with multifunctionality, trimetallic AuPtPd mesoporous nanospheres were rationally designed by virtue of the synergistic effect of different noble metals. Moreover, BiVO_4 was chosen as the photoactive material to guarantee a remarkable photocurrent resulting from its good light-harvesting ability. The morphologies and structures of AuPtPd, BiVO_4 , and $\text{BiVO}_4\text{-AuPtPd}$ were investigated utilizing scanning electron microscopy (SEM), X-ray diffraction (XRD), and X-ray photoelectron spectroscopy (XPS). The BiOI electrode was synthesized by electro-deposition, and then annealed in air to prepare the BiVO_4 electrode. According to the digital photographs shown in Figure S2, the successful formation of BiVO_4 photoelectrodes with a typical color was clearly observed. As can be seen from the SEM image (Figure 1A), the as-prepared BiVO_4

photoelectrodes show a nanoporous and worm-like morphology, which favors charge transport. In addition, AuPtPd nanozymes exhibit a relatively uniform size and shape, showing a porous spherical structure with a diameter of about 150 nm (Figure S3). As for $\text{BiVO}_4\text{-AuPtPd}$ (Figure 1B), the morphology of AuPtPd was well maintained and evenly dispersed on BiVO_4 . Furthermore, the elemental composition and spatial distribution were studied by energy-dispersive X-ray (EDX) element mapping analysis (Figure S4). The existence of Bi, V, O, Au, Pt, and Pd was confirmed in the $\text{BiVO}_4\text{-AuPtPd}$ composite material, which demonstrated the successful attachment of AuPtPd onto the surface of BiVO_4 .

XRD was used to analyze the phase structure of these samples (Figure 1C), which indicated the successful synthesis of BiVO_4 (JCPDS14-0688) and trimetallic AuPtPd (Au: JCPDS-04-0784 and JCPDS-04-0784; Pt: JCPDS-04-0802; Pd: JCPDS 46-1043). Noteworthy, the lattice mismatch ratios of Pt/Pd and Pt/Au are 0.77 and 4.08%, respectively. It is difficult to distinguish the peaks of Pt and Pd in the XRD pattern, while the peaks of Au and Pt–Pd can be easily recognized.^{52,56} To further confirm the surface chemical compositions and electronic states, the $\text{BiVO}_4\text{-AuPtPd}$ electrodes were investigated by XPS (Figure 1D). Consistent with the results of EDX element mapping analysis (Figure S5), the general survey XPS further indicated that $\text{BiVO}_4\text{-AuPtPd}$ contained the elements of Bi, V, O, Au, Pt, and Pd. In addition, Figure 1E,F shows the high-resolution XPS spectra of Bi 4f and V 2p, respectively. The peaks located at 159.2, 164.5, 516.6, and 524.2 eV can be assigned to Bi 4f_{7/2}, Bi 4f_{5/2}, V 2p_{3/2}, and V 2p_{1/2}, respectively, and are the characteristic peaks of Bi and V in BiVO_4 .⁵⁷

Then, the PEC activities of the as-prepared photoelectrodes were measured by the instantaneous photocurrent response in 0.1 M PBS (pH 7.0) at a constant potential of 0 V under visible light ($\lambda \geq 420$ nm) irradiation. To alleviate charge recombination, AA was added as an effective hole scavenger to quickly consume holes in BiVO_4 . As shown in Figure 2A, the bare ITO electrode exhibited a negligible photocurrent, while the BiVO_4 and $\text{BiVO}_4\text{-AuPtPd}$ modified electrodes show a relatively strong anodic photocurrent. To optimize the

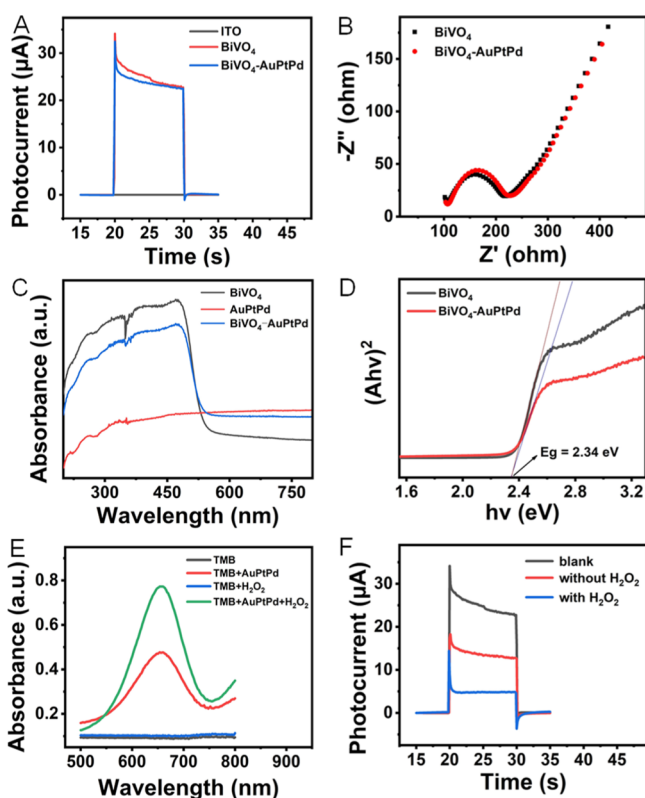


Figure 2. (A) Photocurrent of bare ITO, BiVO_4 , and BiVO_4 -AuPtPd in 0.1 M PBS (pH 7) at 0 V under visible light. (B) EIS Nyquist plots of BiVO_4 and BiVO_4 -AuPtPd in 1 M KCl solution containing 5 mM $[\text{Fe}(\text{CN})_6]^{3-/4-}$. (C) UV-vis diffuse reflectance spectra of BiVO_4 , AuPtPd, and BiVO_4 -AuPtPd. (D) Tauc plots of BiVO_4 and BiVO_4 -AuPtPd. (E) UV-vis absorption spectra of TMB, TMB + AuPtPd, TMB + H_2O_2 , and TMB + AuPtPd + H_2O_2 . (F) The influence of H_2O_2 on photocurrent in the PEC analysis system.

photocurrent of BiVO_4 -AuPtPd, the amounts of AuPtPd nanozymes were studied and a concentration of 0.2 mg mL^{-1} was selected as the optimal concentration for the following experiment (Figure S6A). As a result, AuPtPd nanozymes exhibit a slight effect on the photocurrent of BiVO_4 . In addition, the superior stability of photocurrent based on BiVO_4 -AuPtPd photoactive materials under 400 s on/off light irradiation has also been verified (Figure S6B).

EIS measurement was employed to further investigate the influence of AuPtPd nanozymes on the charge-transfer resistance of the photoelectrode.⁵⁸ Generally speaking, the Nyquist graph is composed of a semicircle and a linear part.¹³ Among them, the semicircle diameter represents the R_{ct} value between the interface of the electrode and the electrolyte. As shown in Figure 2B, the R_{ct} value of BiVO_4 -AuPtPd was changeless compared with that of BiVO_4 , indicating that the introduction of AuPtPd nanozymes has no effect on the charge transfer.

The light absorption properties of BiVO_4 , AuPtPd, and BiVO_4 -AuPtPd were measured with the UV-vis diffuse reflectance (Figure 2C). As expected, AuPtPd nanozymes with metallic properties exhibit no obvious absorption edge, while the absorption edges of both the BiVO_4 and BiVO_4 -AuPtPd samples are about 520 nm. The band gap energies (E_g) of both BiVO_4 and BiVO_4 -AuPtPd were almost unchanged, which were 2.34 eV (Figure 2D). According to the Mott-Schottky curve of BiVO_4 , the tangent slope is positive,

indicating the n-type characteristic of BiVO_4 . In addition, the flat band potential (E_{fb}) can be obtained as 0.28 eV according to the intercept on the abscissa (Figure S7).

Evaluation of Oxidase and Peroxidase-like Activities of AuPtPd Nanozymes.

The oxidase and peroxidase-like activities of AuPtPd nanozymes were investigated with a typical chromogenic reaction, during which the oxidation of TMB into oxTMB was triggered with or without H_2O_2 . As shown in Figure 2E, in the presence of AuPtPd and TMB, a strong absorption peak was observed at 652 nm. After further addition of H_2O_2 , the absorption peak intensity at 652 nm increased, while no distinct color change was observed for the individual TMB or TMB + H_2O_2 system, demonstrating the superb oxidase and peroxidase-like features of AuPtPd mesoporous spheres. Owing to the oxidase and peroxidase-like activities of AuPtPd nanozymes, the oxidation of 4-CN would be catalyzed to form insoluble benzo-4-chlorohexadienone (4-CD) precipitates on the photoelectrode surface, leading to a large interfacial resistance and a suppressed photocurrent. As exhibited in Figure 2F, a significant variation in the photocurrent could be realized upon the addition of H_2O_2 , demonstrating the advantages of multifunctional nanozymes in synergistic signal amplification. Inspired by the proton-dependent regulatory mechanism for natural enzymes, the pH-regulated catalytic activities of AuPtPd nanozymes were investigated. As depicted in Figure S8A,B, the superb oxidase and peroxidase-like properties of AuPtPd nanozymes were achieved at a pH value of 4, and their activities decayed rapidly when the concentration of protons decreased. Therefore, the oxidase and peroxidase-like activities of AuPtPd nanozymes can be rationally tailored by proton-consuming enzyme-catalyzed bioreactions, which in turn influence the formation of bioprecipitation via the oxidation of 4-CN and subsequently alter the photoresponse and R_{ct} of the photoelectrode. To better understand the oxidase-like activity of AuPtPd nanozymes, the steady-state kinetics was investigated. Typical Michaelis-Menten curves for AuPtPd nanozymes were obtained over a certain range of TMB concentrations (Figure S9). The K_m and V_{max} values of AuPtPd nanozymes were determined to be 6.28 mM and $3.41 \times 10^{-7} \text{ M s}^{-1}$ for TMB, respectively.

Performance of the Dual-Modal Biosensor for Urease Detection.

Urease, as a typical proton-consuming enzyme, can catalyze the decomposition of urea to produce ammonia, making it feasible to modulate the catalytic activities of AuPtPd nanozymes and achieve the dual-modal detection of urease activity. First, the reaction time and temperature were optimized to guarantee the best catalytic activity of urease (Figure S10A,B) and AuPtPd nanozymes (Figure S11A,B), and a reaction time of 30 min and a reaction temperature of 37°C were chosen as the optimal conditions.

As shown in Figure 3A, the photocurrent of the pristine BiVO_4 -AuPtPd photoelectrode is $22.5 \mu\text{A}$. In the absence of urease, no proton was consumed, and AuPtPd nanozymes exhibited the best activity to catalyze the oxidation of 4-CN into 4-CD precipitation to significantly inhibit the photocurrent (Figure 3A). However, the catalytic activity of AuPtPd nanozymes will be depressed and a higher photocurrent was observed along with the proton-consuming bioreaction in the presence of urease ($C_{\text{urease}} = 160 \text{ mU mL}^{-1}$) (Figure 3A). Therefore, it can be concluded that the pH-regulated PEC performance of the BiVO_4 -AuPtPd photoelectrode was suitable for the sensitive detection of urease. Figure 3B

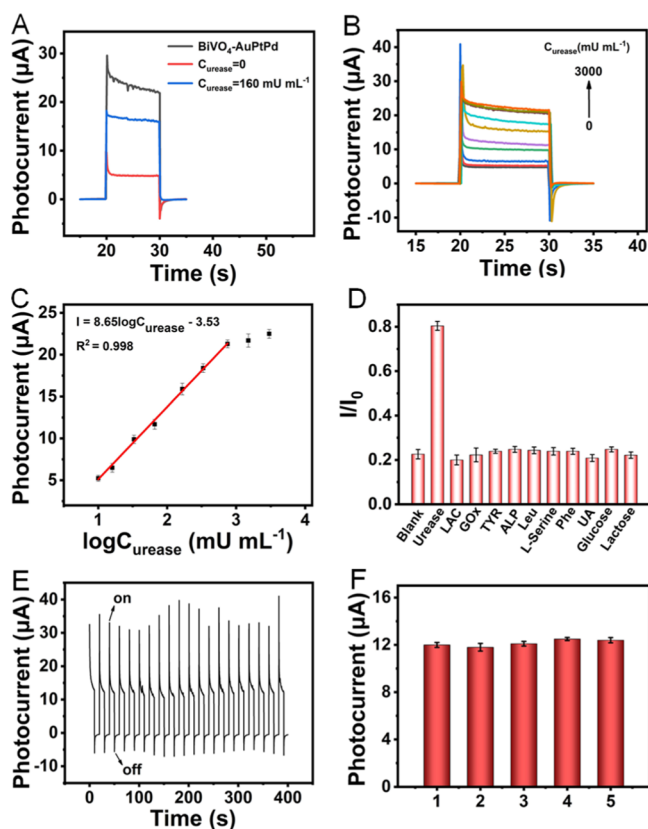


Figure 3. (A) Photocurrent response of the pristine BiVO₄-AuPtPd and BiVO₄-AuPtPd photoelectrodes incubated at various concentrations of urease (0 and 160 mU mL⁻¹). (B) Photocurrent of the PEC sensing system with different concentrations of urease (0, 10, 15, 30, 60, 160, 320, 750, 1500, and 3000 mU mL⁻¹). (C) A linear plot of photocurrent response versus the logarithm of the urease concentration (10–750 mU mL⁻¹). (D) Selectivity of the PEC biosensor for urease detection ($C_{\text{urease}} = 60 \text{ mU mL}^{-1}$, I_0 is the initial photocurrent responses of BiVO₄-AuPtPd). (E) Time-based photocurrent responses of the PEC sensing system ($C_{\text{urease}} = 60 \text{ mU mL}^{-1}$) with light on and off. (F) Repeatability of a PEC sensor ($C_{\text{urease}} = 60 \text{ mU mL}^{-1}$).

presents the photocurrents of the BiVO₄-AuPtPd-based PEC sensing system toward different concentrations of urease (10–3000 mU mL⁻¹). As expected, the photocurrent of BiVO₄-AuPtPd photoelectrodes gradually increases along with the continuously increasing urease concentration, while it remains almost changeless at higher concentrations than 750 mU mL⁻¹ (Figure 3B). As a result, the linear relationship between the PEC response and the logarithm of the urease concentration was realized in the range of 10–750 mU mL⁻¹ (Figure 3C), which can be described using the formula of $I (\mu\text{A}) = 8.65 \log C_{\text{urease}} - 3.53$ ($R^2 = 0.998$). The limit of detection (LOD, $S/N = 3$) was calculated to be 8.4 mU mL⁻¹.

To evaluate the selectivity of the as-prepared PEC biosensor for urease, the photocurrent responses toward some other potentially common compounds that may be present in samples were investigated. Common biomolecules such as uric acid, lactose, and glucose (50 μM), amino acids such as leucine, L-serine, and phenylalanine (50 μM), and biological enzymes such as laccase, glucose oxidase, tyrosinase, and alkaline phosphatase (2000 mU mL⁻¹) were selected as interferers. As displayed in Figure 3D, the effect of the added interferers is ignorable compared with the significant

photocurrent change induced by urease, which indicated the good selectivity of the BiVO₄-AuPtPd-based PEC sensing platform for the urease detection. In addition, the stability (Figure 3E) for 400 s of switching light irradiation and the reproducibility (Figure 3F) of the prepared PEC biosensor were studied at a urease concentration of 60 mU mL⁻¹. Notably, the photocurrents were almost constant during the measurements, which indicates the satisfactory stability and reproducibility of the sensor.

We also further verified the feasibility of detecting urease through the EIS method. The experimental procedure was similar to the PEC sensing system for urease. As shown in Figure 4A, the Nyquist plot of the pristine BiVO₄-AuPtPd

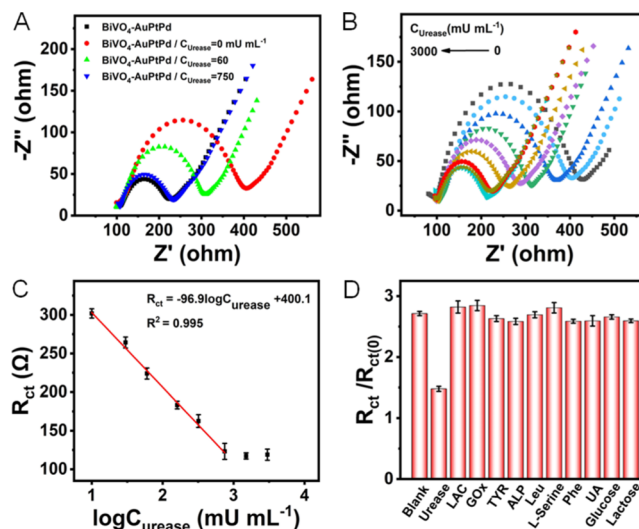


Figure 4. (A) EIS Nyquist plots of the BiVO₄-AuPtPd photoelectrode with various concentrations of urease (0, 60, and 750 mU mL⁻¹) in 1 M KCl solution containing 5 mM [Fe(CN)₆]^{3-/4-}. (B) EIS Nyquist plots of the BiVO₄-AuPtPd photoelectrode with various concentrations of urease (0, 10, 30, 60, 160, 320, 750, 1500, and 3000 mU mL⁻¹). (C) A linear plot of R_{ct} versus the logarithm of the urease concentration (10–750 mU mL⁻¹). (D) Selectivity of the biosensor for urease (160 mU mL⁻¹) detection (R_{ct} is the initial charge-transfer resistance of BiVO₄-AuPtPd).

photoelectrode displays a small semicircle with an R_{ct} value of about 120 Ω (black curve). In the absence of urease, the largest R_{ct} was observed, which was in accordance with its smallest photocurrent. As expected, the R_{ct} value decreased significantly with the increase of concentrations of urease. Notably, the R_{ct} value of BiVO₄-AuPtPd photoelectrodes gradually decreased along with the continuously increasing urease concentration, which remains almost constant at higher concentrations than 750 mU mL⁻¹ (Figure 4B).

As a result, the linear relationship between the R_{ct} value and the logarithm of the urease concentration was realized in the range of 10–750 mU mL⁻¹ (Figure 4C), which can be described by the formula $R_{\text{ct}} (\mu\text{A}) = -96.9 \log C_{\text{urease}} + 400.1$ ($R^2 = 0.995$). The LOD was calculated to be 6.6 mU mL⁻¹. Similarly, the R_{ct} inhibition from several interferers is ignorable in contrast with urease, which declares the excellent selectivity of the proposed biosensor based on BiVO₄-AuPtPd. Notably, Table S1 shows the comparison of our results with those of the previously reported method for the determination of urease, indicating that the results obtained

using the biosensor based on the BiVO₄–AuPtPd photoelectrode are among the best-known results.

Furthermore, the applicability of this urease sensing system was assessed in the human saliva samples by the standard addition method. The recovery tests were performed, and the relative standard deviations (RSDs) were acquired from three samples. As shown in Table 1, the recoveries varied from 96.0

Table 1. Determination of Urease in Human Saliva Samples

sample	spiked (mU mL ⁻¹)	found (mU mL ⁻¹)	recovered (%)	RSD (%)
I	10.0	9.6 ± 0.07	96.0	3.73
II	100.0	97.5 ± 0.47	97.5	3.16
III	500.0	507.2 ± 1.65	101.4	1.42

to 101.4% and the RSDs ranged from 1.42 to 3.73%, indicating the reliability of the biosensor and its potential application in clinical diagnosis. Moreover, urease with concentrations of 20, 50, 100, 200, and 500 mU mL⁻¹ were selected to study the PEC and EC performance of the system. The test procedure was the same as the previous procedure for measuring urease activity. The resulting photocurrent value was substituted into the linear equation to obtain the urease concentration. A good linear correlation ($R^2 = 0.992$) was observed between the results obtained from the PEC and the EC method (Figure S12), indicating the acceptable reliability and accuracy of the dual-modal biosensor.

CONCLUSIONS

In this work, multifunctional AuPtPd nanozymes were reasonably designed and synthesized with outstanding oxidase and peroxide-like activities. Based on the urease-mediated proton-consuming enzymatic reactions, a dual-modal PEC and EC biosensor for the evaluation of urease activity was innovatively constructed by in situ regulating the synergistic catalytic activity of AuPtPd nanozymes. Based on these strategies, the as-prepared biosensor shows excellent selectivity, good repeatability, and high stability. Meanwhile, the determination of urease activity in spiked human saliva samples was successfully realized, indicating the reliability of the biosensor and its application prospects in clinical diagnosis. This work sheds light on the superiority of multifunctional nanozymes in synergistic amplification and opens up a new avenue for building a sensitive biosensing platform with nanozymes.

ASSOCIATED CONTENT

Supporting Information

The Supporting Information is available free of charge at <https://pubs.acs.org/doi/10.1021/acs.analchem.1c01999>.

Materials and reagents; instrument; current–time curve for electrodeposition of BiOI; digital images of the BiOI and BiVO₄ photoelectrodes; SEM image of AuPtPd; elemental mapping images of BiVO₄–AuPtPd; EDX element mapping analysis; effect of AuPtPd on the photocurrent of BiVO₄–AuPtPd; PEC stability of the BiVO₄–AuPtPd electrode; Mott–Schottky curve of BiVO₄; oxidase and peroxidase-like activities of the AuPtPd nanozymes; steady-state kinetic assay of TMB oxidation by AuPtPd nanozymes; optimum reaction time and temperature for urease incubation in a 96-well plate; optimal reaction time and temperature for urease

detection by PEC; comparison of the results obtained from the two methods of PEC and EC; and comparison of different methods for urease detection (PDF)

AUTHOR INFORMATION

Corresponding Authors

Liuyong Hu – Hubei Engineering Technology Research Center of Optoelectronic and New Energy Materials, Hubei Key Laboratory of Plasma Chemistry and Advanced Materials, School of Materials Science and Engineering, Wuhan Institute of Technology, Wuhan 430205, P. R. China; Email: huly@wit.edu.cn

Wenling Gu – Key Laboratory of Pesticide and Chemical Biology of Ministry of Education, International Joint Research Center for Intelligent Biosensing Technology and Health, College of Chemistry, Central China Normal University, Wuhan 430079, P. R. China; Email: wlg@mail.ccnu.edu.cn

Chengzhou Zhu – Key Laboratory of Pesticide and Chemical Biology of Ministry of Education, International Joint Research Center for Intelligent Biosensing Technology and Health, College of Chemistry, Central China Normal University, Wuhan 430079, P. R. China; orcid.org/0000-0003-0679-7965; Email: czzhu@mail.ccnu.edu.cn

Authors

Mingwang Liu – Key Laboratory of Pesticide and Chemical Biology of Ministry of Education, International Joint Research Center for Intelligent Biosensing Technology and Health, College of Chemistry, Central China Normal University, Wuhan 430079, P. R. China

Guojuan Chen – Key Laboratory of Pesticide and Chemical Biology of Ministry of Education, International Joint Research Center for Intelligent Biosensing Technology and Health, College of Chemistry, Central China Normal University, Wuhan 430079, P. R. China

Ying Qin – Key Laboratory of Pesticide and Chemical Biology of Ministry of Education, International Joint Research Center for Intelligent Biosensing Technology and Health, College of Chemistry, Central China Normal University, Wuhan 430079, P. R. China

Jinli Li – Key Laboratory of Pesticide and Chemical Biology of Ministry of Education, International Joint Research Center for Intelligent Biosensing Technology and Health, College of Chemistry, Central China Normal University, Wuhan 430079, P. R. China

Complete contact information is available at:

<https://pubs.acs.org/doi/10.1021/acs.analchem.1c01999>

Notes

The authors declare no competing financial interest.

ACKNOWLEDGMENTS

The authors gratefully acknowledge the financial support by the National Natural Science Foundation of China (nos. 22074049 and 22004042), the Natural Science Foundation of Hubei Province (2020CFB276), the Fundamental Research Funds for the Central Universities (nos. CCNU20QN007 and CCNU20TS013), and the Program of Introducing Talents of Discipline to Universities of China (111 program, B17019).

REFERENCES

- (1) Dixon, N. E.; Gazzola, C.; Blakeley, R. L.; Zerner, B. J. *Am. Chem. Soc.* **1975**, *97*, 4131–4133.
- (2) Mobley, H. L.; Island, M. D.; Hausinger, R. P. *Microbiol. Rev.* **1995**, *59*, 451–480.
- (3) Krajewska, B. J. *Mol. Catal. B: Enzym.* **2009**, *59*, 9–21.
- (4) Follmer, C. J. *Clin. Pathol.* **2010**, *63*, 424–430.
- (5) Rechenmacher, C.; Wiebke-Strohm, B.; Oliveira-Busatto, L. A. d.; Polacco, J. C.; Carlini, C. R.; Bodanese-Zanettini, M. H. *Genet. Mol. Biol.* **2017**, *40*, 209–216.
- (6) Hu, S.; Gao, Y.; Wu, Y.; Guo, X.; Ying, Y.; Wen, Y.; Yang, H. *Biosens. Bioelectron.* **2019**, *129*, 24–28.
- (7) Wang, M.; Wang, S.; Song, X.; Liang, Z.; Su, X. *Sens. Actuators, B* **2020**, *316*, 128157.
- (8) Patten, B. E.; Higgins, P. A.; Whithear, K. G. *Aust. Vet. J.* **1984**, *61*, 151–155.
- (9) Lonsdale, W.; Maurya, D. K.; Wajrak, M.; Tay, C. Y.; Marshall, B. J.; Alameh, K. *Sens. Actuators, B* **2017**, *242*, 1305–1308.
- (10) Deng, H.-H.; Wu, G.-W.; Zou, Z.-Q.; Peng, H.-P.; Liu, A.-L.; Lin, X.-H.; Xia, X.-H.; Chen, W. *Chem. Commun.* **2015**, *51*, 7847–7850.
- (11) Li, L.; Long, Y.; Gao, J.-M.; Song, K.; Yang, G. *Nanoscale* **2016**, *8*, 4458–4462.
- (12) Chu, Y.; Deng, A.-P.; Wang, W.; Zhu, J.-J. *Anal. Chem.* **2019**, *91*, 3619–3627.
- (13) Fan, G.-C.; Zhu, H.; Du, D.; Zhang, J.-R.; Zhu, J.-J.; Lin, Y. *Anal. Chem.* **2016**, *88*, 3392–3399.
- (14) Hao, N.; Hua, R.; Chen, S.; Zhang, Y.; Zhou, Z.; Qian, J.; Liu, Q.; Wang, K. *Biosens. Bioelectron.* **2018**, *101*, 14–20.
- (15) Li, W.; Fan, G.-C.; Gao, F.; Cui, Y.; Wang, W.; Luo, X. *Biosens. Bioelectron.* **2019**, *127*, 64–71.
- (16) Li, X.; Lu, J.; Feng, L.; Zhang, L.; Gong, J. *Anal. Chem.* **2020**, *92*, 11476–11483.
- (17) Long, D.; Li, M.; Wang, H.; Wang, H.; Chai, Y.; Li, Z.; Yuan, R. *Anal. Chem.* **2020**, *92*, 14769–14774.
- (18) Meng, L.; Xiao, K.; Zhang, X.; Du, C.; Chen, J. *Biosens. Bioelectron.* **2020**, *150*, 111861.
- (19) Tang, Y.; Chai, Y.; Liu, X.; Li, L.; Yang, L.; Liu, P.; Zhou, Y.; Ju, H.; Cheng, Y. *Biosens. Bioelectron.* **2018**, *117*, 224–231.
- (20) Tu, W.; Wang, Z.; Dai, Z. *TrAC, Trends Anal. Chem.* **2018**, *105*, 470–483.
- (21) Wang, Q.; Yin, H.; Zhou, Y.; Wang, J.; Ai, S. *J. Hazard. Mater.* **2021**, *414*, 125293.
- (22) Wei, J.; Hu, Q.; Gao, Y.; Hao, N.; Qian, J.; Wang, K. *Anal. Chem.* **2021**, *93*, 6214–6222.
- (23) Xia, L.-Y.; Li, M.-J.; Wang, H.-J.; Yuan, R.; Chai, Y.-Q. *Anal. Chem.* **2020**, *92*, 14550–14557.
- (24) Xu, M.; Da, P.; Wu, H.; Zhao, D.; Zheng, G. *Nano Lett.* **2012**, *12*, 1503–1508.
- (25) Zhang, K.; Lv, S.; Lin, Z.; Li, M.; Tang, D. *Biosens. Bioelectron.* **2018**, *101*, 159–166.
- (26) Zhang, N.; Ma, Z.-Y.; Ruan, Y.-F.; Zhao, W.-W.; Xu, J.-J.; Chen, H.-Y. *Anal. Chem.* **2016**, *88*, 1990–1994.
- (27) Zhang, X. Y.; Liu, S. G.; Zhang, W. J.; Wang, X. H.; Han, L.; Ling, Y.; Li, N. B.; Luo, H. Q. *Sens. Actuators, B* **2019**, *297*, 126818.
- (28) Zhao, W.-W.; Xu, J.-J.; Chen, H.-Y. *Chem. Rev.* **2014**, *114*, 7421–7441.
- (29) Qin, Y.; Wen, J.; Zheng, L.; Yan, H.; Jiao, L.; Wang, X.; Cai, X.; Wu, Y.; Chen, G.; Chen, L.; Hu, L.; Gu, W.; Zhu, C. *Nano Lett.* **2021**, *21*, 1879–1887.
- (30) Shu, J.; Tang, D. *Anal. Chem.* **2020**, *92*, 363–377.
- (31) Zhou, Q.; Tang, D. *TrAC, Trends Anal. Chem.* **2020**, *124*, 115814.
- (32) Zhao, W.-W.; Xu, J.-J.; Chen, H.-Y. *Anal. Chem.* **2018**, *90*, 615–627.
- (33) Qian, Y.; Feng, J.; Fan, D.; Zhang, Y.; Kuang, X.; Wang, H.; Wei, Q.; Ju, H. *Biosens. Bioelectron.* **2019**, *131*, 299–306.
- (34) Zhu, C.; Yang, G.; Li, H.; Du, D.; Lin, Y. *Anal. Chem.* **2015**, *87*, 230–249.
- (35) Wang, H.; Yin, H.; Huang, H.; Li, K.; Zhou, Y.; Waterhouse, G. I. N.; Lin, H.; Ai, S. *Biosens. Bioelectron.* **2018**, *108*, 89–96.
- (36) Wang, B.; Dong, Y.-X.; Wang, Y.-L.; Cao, J.-T.; Ma, S.-H.; Liu, Y.-M. *Biosens. Bioelectron.* **2018**, *254*, 159–165.
- (37) Yang, R.; Zou, K.; Li, Y.; Meng, L.; Zhang, X.; Chen, J. *Anal. Chem.* **2018**, *90*, 9480–9486.
- (38) Zhao, W.-W.; Ma, Z.-Y.; Yu, P.-P.; Dong, X.-Y.; Xu, J.-J.; Chen, H.-Y. *Anal. Chem.* **2012**, *84*, 917–923.
- (39) Jiao, L.; Xu, W.; Wu, Y.; Yan, H.; Gu, W.; Du, D.; Lin, Y.; Zhu, C. *Chem. Soc. Rev.* **2021**, *50*, 750–765.
- (40) Jiao, L.; Xu, W.; Yan, H.; Wu, Y.; Liu, C.; Du, D.; Lin, Y.; Zhu, C. *Anal. Chem.* **2019**, *91*, 11994–11999.
- (41) Wu, Y.; Wu, J.; Jiao, L.; Xu, W.; Wang, H.; Wei, X.; Gu, W.; Ren, G.; Zhang, N.; Zhang, Q.; Huang, L.; Gu, L.; Zhu, C. *Anal. Chem.* **2020**, *92*, 3373–3379.
- (42) Wu, Y.; Jiao, L.; Luo, X.; Xu, W.; Wei, X.; Wang, H.; Yan, H.; Gu, W.; Xu, B. Z.; Du, D.; Lin, Y.; Zhu, C. *Small* **2019**, *15*, 1903108.
- (43) Wei, H.; Wang, E. *Chem. Soc. Rev.* **2013**, *42*, 6060–6093.
- (44) Wu, J.; Wang, X.; Wang, Q.; Lou, Z.; Li, S.; Zhu, Y.; Qin, L.; Wei, H. *Chem. Soc. Rev.* **2019**, *48*, 1004–1076.
- (45) Gong, L.; Dai, H.; Zhang, S.; Lin, Y. *Anal. Chem.* **2016**, *88*, 5775–5782.
- (46) Jiao, L.; Yan, H.; Wu, Y.; Gu, W.; Zhu, C.; Du, D.; Lin, Y. *Angew. Chem., Int. Ed.* **2020**, *59*, 2565–2576.
- (47) Li, F.; Zhou, Y.; Wang, S.; Yin, H.; Chen, Y.; Luo, H.; Ai, S. *Biosens. Bioelectron.* **2020**, *151*, 111973.
- (48) Huang, D.; Wang, L.; Zhan, Y.; Zou, L.; Ye, B. *Biosens. Bioelectron.* **2019**, *140*, 111358.
- (49) Cheng, H.; Lin, S.; Muhammad, F.; Lin, Y.-W.; Wei, H. *ACS Sens.* **2016**, *1*, 1336–1343.
- (50) Wang, X.; Gao, X. J.; Qin, L.; Wang, C.; Song, L.; Zhou, Y.-N.; Zhu, G.; Cao, W.; Lin, S.; Zhou, L.; Wang, K.; Zhang, H.; Jin, Z.; Wang, P.; Gao, X.; Wei, H. *Nat. Commun.* **2019**, *10*, 704.
- (51) Li, C.; Wang, H.; Li, Y.; Yu, H.; Yin, S.; Xue, H.; Li, X.; Xu, Y.; Wang, L. *Nanotechnology* **2018**, *29*, 255404.
- (52) Wang, L.; Yamauchi, Y. *J. Am. Chem. Soc.* **2010**, *132*, 13636–13638.
- (53) Jiang, B.; Li, C.; Imura, M.; Tang, J.; Yamauchi, Y. *Adv. Sci.* **2015**, *2*, 1500112.
- (54) Asati, A.; Santra, S.; Kaittanis, C.; Nath, S.; Perez, J. M. *Angew. Chem., Int. Ed.* **2009**, *48*, 2308–2312.
- (55) Yan, D.; Fu, X.; Shang, Z.; Liu, J.; Luo, H. a. *Chem. Eng. J.* **2019**, *361*, 853–861.
- (56) Lim, B.; Jiang, M.; Camargo, P. H. C.; Cho, E. C.; Tao, J.; Lu, X.; Zhu, Y.; Xia, Y. *Science* **2009**, *324*, 1302–1305.
- (57) Zhang, B.; Wang, L.; Zhang, Y.; Ding, Y.; Bi, Y. *Angew. Chem., Int. Ed.* **2018**, *57*, 2248–2252.
- (58) Feng, C.; Tang, L.; Deng, Y.; Zeng, G.; Wang, J.; Liu, Y.; Chen, Z.; Yu, J.; Wang, J. *Appl. Catal., B* **2019**, *256*, 117827.